

Supplemental Data

Development of CD11b-IRF8 transgenic and MTAG double transgenic mice The CMV-IRF8 transgenic mouse was previously developed by cloning complementary DNA, containing the IRF-8 coding sequence, into pcDNA3.1+ under control of the CMV promoter (24). To produce the CD11b-IRF8 transgenic mouse, we replaced the CMV promoter and transcription initiation region with the murine CD11b promoter and accompanying transcription initiation region. Using the genomic DNA purified from normal mouse cells, the mouse CD11b promoter (-2000 to -1), including the 5'-untranslated region was amplified by PCR. Following subcloning, the resultant 4.3 kb fragment, which contained the functional transcriptional unit (i.e., promoter, gene, poly A sites) was purified and then microinjected into the pronuclei of one cell embryos of fertilized eggs from B6 mice to obtain several founder mice. Transgene integration in progeny was verified by Southern blot analysis using the 4.3 kb fragment as the probe and PCR genotyping of tail snips.

Progeny for experimental studies were produced by mating IRF-8-Tg male mice with either wild-type female B6 or BALB/c mice. The founder lines, 370 and 371, were selected for this study based on the highest IRF-8 copy number and mRNA levels and in initial experiments both behaved similarly in their ability to attenuate MDSC effects. No atypical effects of IRF-8 transgene expression were observed on diverse hematologic parameters, including phenotypic analysis of the spleen, complete blood count (CBC) on peripheral whole blood and morphologic analyses of the bone marrow (see Supplemental Figure 2 and Table IV). To develop double-Tg mice expressing transgenes for both MTAG and IRF-8, male MTAG mice were bred with female CD11b-IRF8 Tg mice. To ensure that the transgenes for both IRF-8 and spontaneous mammary

carcinoma development (i.e., MMTV-PyMT) were expressed, PCR analysis for IRF-8 and MTAG expression of tail snip DNA was conducted using the conditions mentioned in the PCR/RT-PCR section below. For simplicity, single-Tg refers to MTAG mice, whereas double-Tg refers to MTAG/CD11b-IRF8 Tg mice.

Molecular analyses. RNA was isolated using RNeasy Mini kits (Qiagen; Valencia, CA). cDNA was synthesized using the iScript cDNA synthesis kit (Bio-Rad, Hercules, CA). The cDNA was then used for RT-PCR and qPCR analysis. RT-PCR was conducted on a PTC-200 thermal cycler (MJ Research, Waltham, MA) under the following standard conditions: 94°C for 2 min, 30 cycles (94°C for 30 sec, 60°C for 30 sec and 72°C for 1 min) and 72°C for 10 min. The following mouse primer sets were used: GAPDH forward: 5'-CATCACCATCTTCC AGGAGCG-3' and reverse: 5'-ACGGACACATTGGGGGTAGG -3', IRF-8 forward: 5'-CGTGG AAGACGAGGTTACGCTG-3'; reverse: 5'-GCTGAATGGTGTGTGTCATAGGC-3'; C/EBP β forward: 5'-AGCCCCTACCTGGAGCCGCTCGCG-3' and reverse: 5'-GCGCAGGGCGAACGGGAAACCG-3'. All qPCR reactions were conducted on an ABI PRISM 7900HT Sequence Detection System (Applied Biosciences, Carlsbad, CA) using RT² SYBR Green mastermix (Qiagen, Valencia, CA). The following primer sets were used for qPCR: IRF-8 forward 5'-TGGAAGCATCCACCTCCTGATTGT-3' and reverse 5'-TGATCGAACAGATCG ACAGCAGCA-3'; GAPDH as previously indicated.

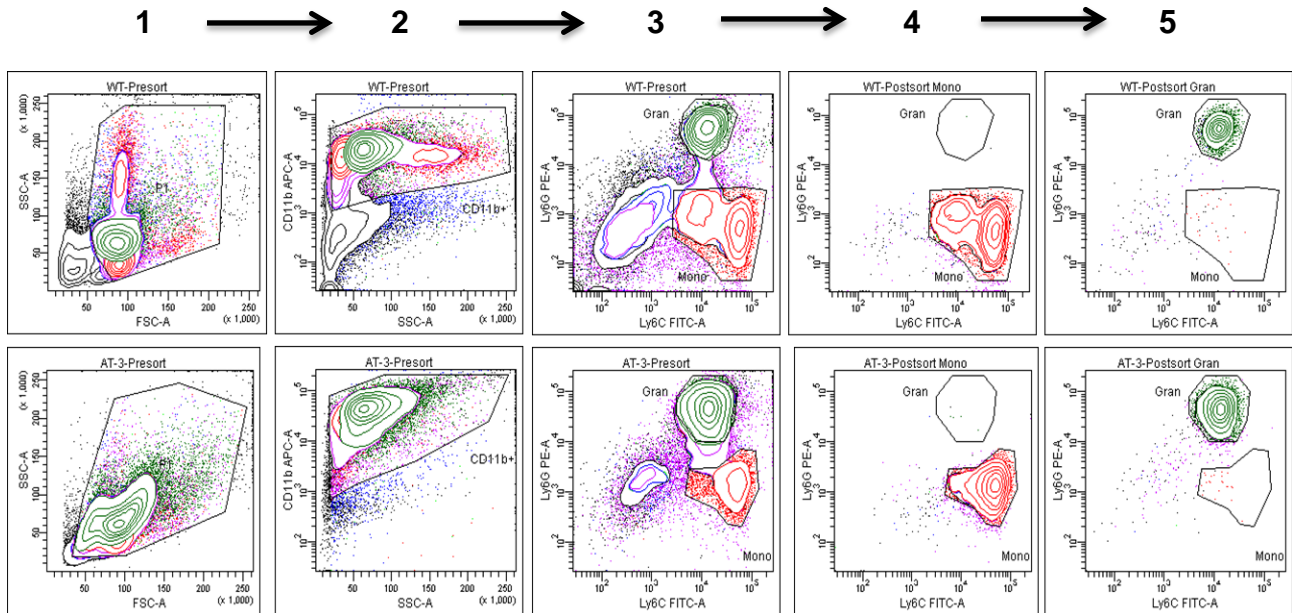
For genotyping, genomic DNA was extracted from tail tissue using DirectPCR tail digestion (Viagen, Los Angeles, CA). MTAG transgene expression was determined using the forward: 5'-AGTCACTGCTACTGCACCCAG-3' and reverse: 5'-CTCTCCTCAGTTCCTCGC

TCC-3' primer set. For IRF-8^{-/-} mice, genotyping was determined using the following primers: 5'-CATGGCACTGGTCCAGATGTCTTCC-3', 5'-CTTCCAGGGATACGGAACATG GTC-3' and 5'-CGAAGGAGCAAAGCTGCTATTGGCC. PCR products were separated on a 1% agarose gel and the images captured with the Chemidoc Imaging System (BioRad).

For the ChIP studies, STAT3 occupation of the IRF-8 promoter was determined using the following primer set (-1398 to -1223); forward 5'-ACTGGGTGGACATTTGGGATCTGT-3' and reverse 5'-AAGTGTTTGCTGTGAAGGGCAGAG-3'. STAT5 occupation of the IRF-8 promoter was analyzed using the following primer set (-677 to -372): forward 5'-CTGCAACGAAAGTCCCTCTC-3' and reverse 5'-CTGAGTGTCAGCTGCTCAGG-3'.

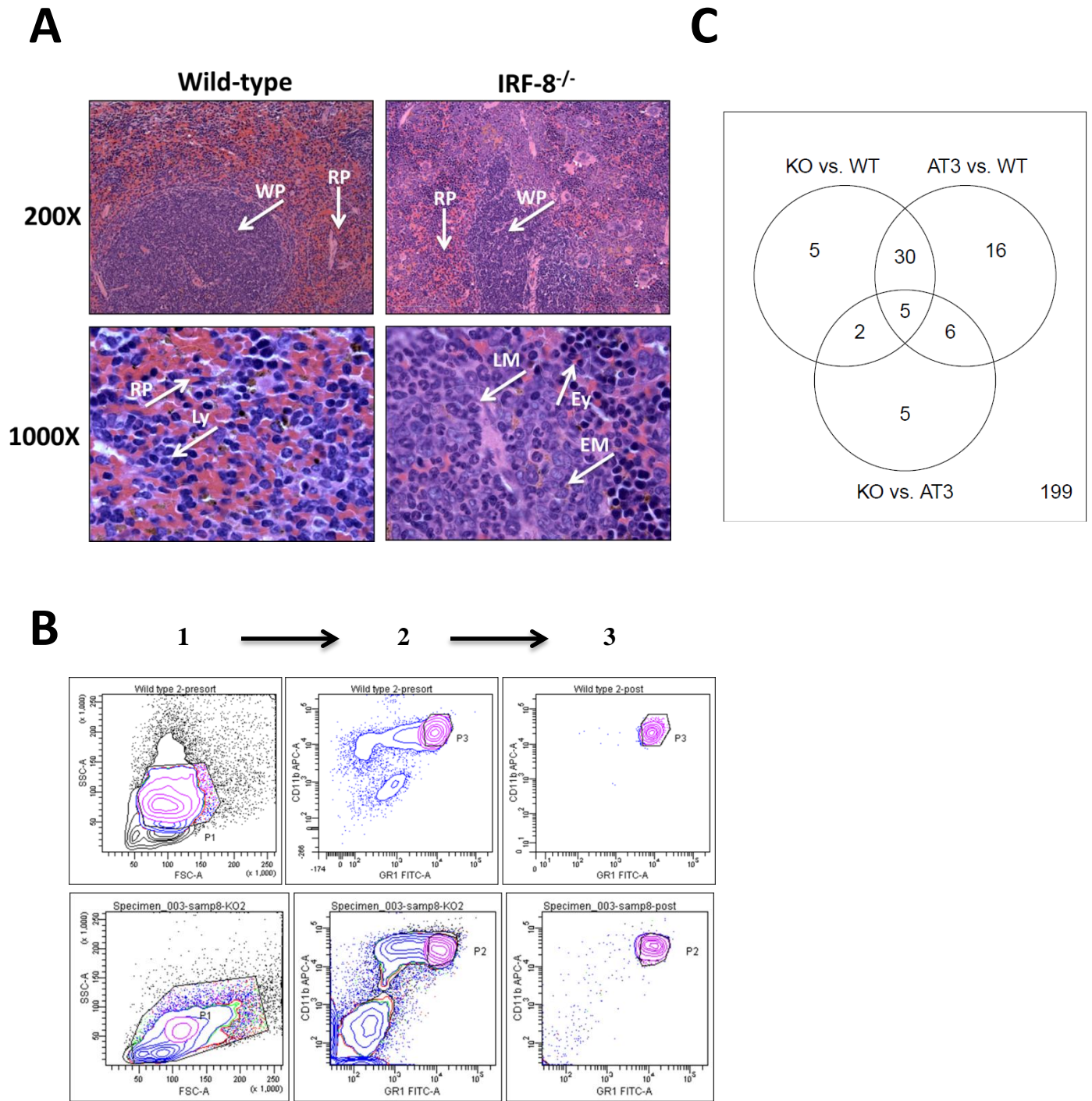
Microarray analysis. Total RNA of flow-purified CD11b⁺ Gr-1⁺ cells from naïve B6, IRF-8^{-/-} or AT-3 tumor-bearing mice (~1500 mm³) was extracted and quantified using a ND-1000 spectrophotometer (NanoDrop, Thermo Scientific). Quality control and direct hybridization to the MouseWG-6 whole-genome gene expression array was conducted and analyzed, as described.³⁰ All data is MIAME compliant.

Supplemental Figures



Supplemental Figure 1. Gating strategy for purification of the different MDSC subsets

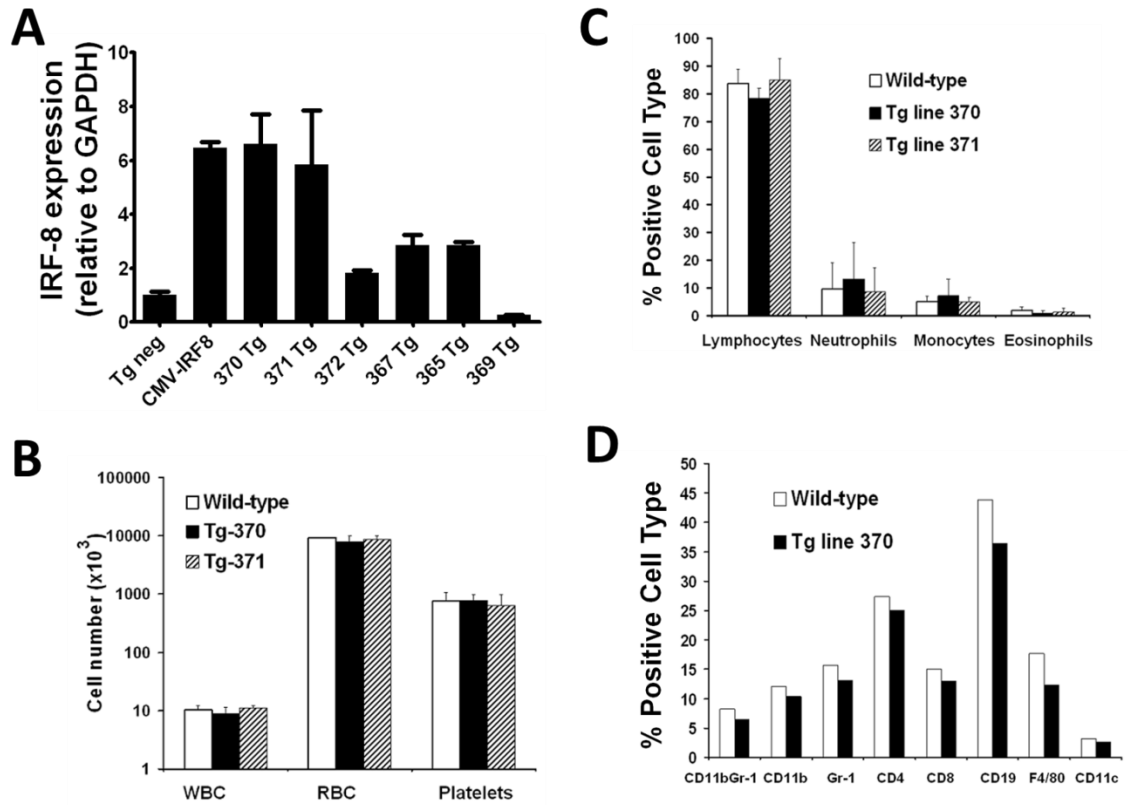
Upper, non-tumor-bearing control mice; *lower*, AT-3 tumor-bearing mice. Splenocytes from the indicated groups of mice were collected and enriched for CD11b⁺ cells using magnetic bead separation methods. Cells from each group were then triple-stained for CD11b (APC), Ly6C (FITC) and Ly6G (PE) expression prior to flow sorting. Next, 1) live cell gate was established; 2) live cells were gated on the CD11b⁺ fraction; 3) gated CD11b⁺ fraction was plotted in relation to Ly6C and Ly6G expression to identify the two non-overlapping subsets prior to sorting; 4) post-sort collection of the CD11b⁺Ly6G⁺Ly6C⁺ monocytic fraction; and 5) post-sort collection of the CD11b⁺Ly6G⁺Ly6C^{lo} granulocytic fraction. In all cases, cell purity was > 97% for the intended subset with < 0.3% contamination of the opposing subset.



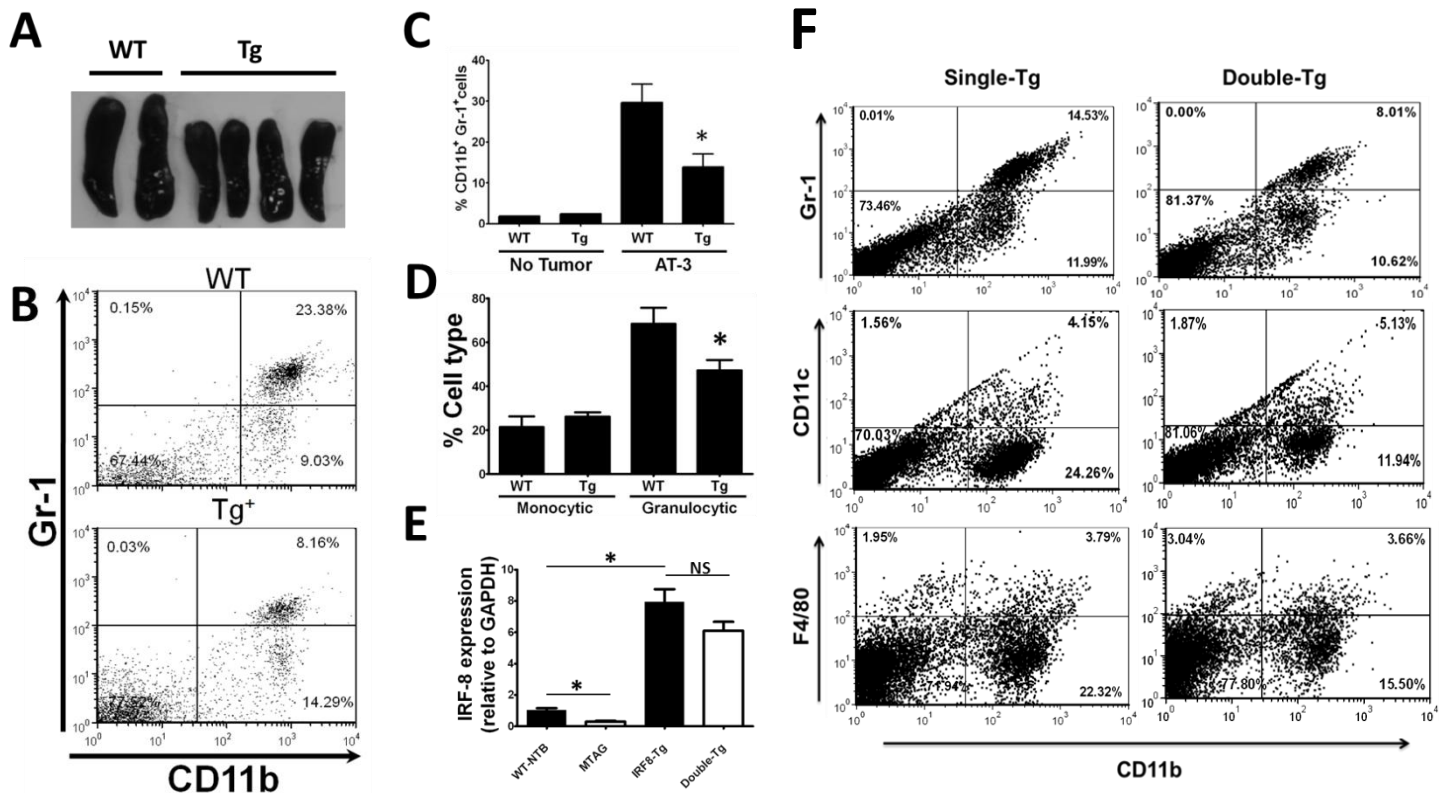
Supplemental Figure 2. IRF-8-deficiency results in the accumulation of MDSC-like cells.

(A) H&E staining of spleens of IRF-8^{-/-} (age=194 days) and WT (age=174 days) mice. One of

two mice for each genotype is shown. Splens of IRF-8^{-/-} mice reveals increased extra-medullary hematopoiesis (EMT) compared to WT mice. Arrows indicate areas of white pulp (WP), red pulp (RP), lymphocytes (Ly), erythroid (Ey) or early (EM) or late (LM) myeloid populations (megakaryocytes, not shown in this image). (B) Gating strategy for the isolation of the CD11b⁺Gr-1^{hi} fraction from splens of WT or IRF-8^{-/-} mice. To do so, 1) live cell gate was established on CD11b-pre-enriched fraction; 2) cells were analyzed for and gated on the CD11b⁺Gr-1^{hi} fraction prior to sorting; and 3) post-sort collection of the CD11b⁺Gr-1^{hi} granulocytic fraction. Cell purities were similar to those of Supplemental Figure 1. Post-sort reveals recovery of phenotypically similar cell populations between both groups. (C) Venn diagram of significantly enriched pathways among the three groups of comparisons.

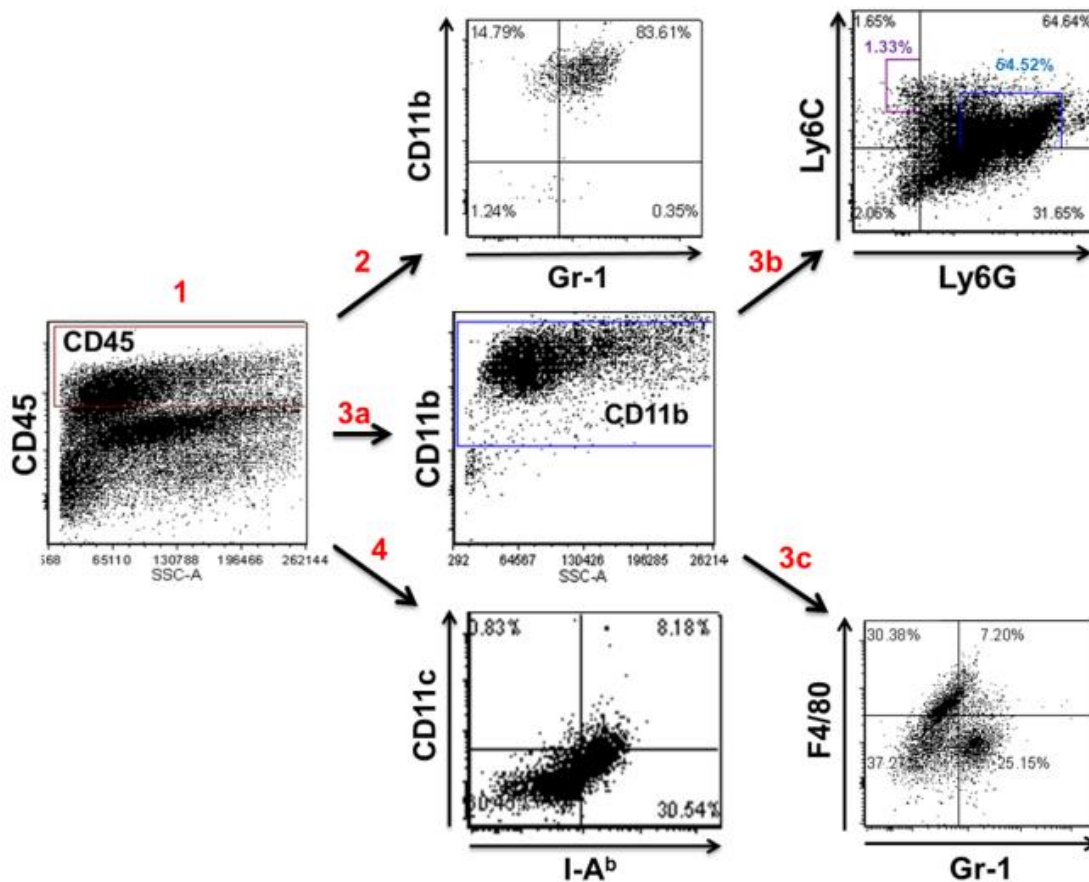


Supplemental Figure 3. Characteristics of the IRF-8 transgenic mouse model. (A) IRF-8 mRNA levels were quantified by qPCR using purified CD11b⁺Gr-1⁺ cells (8 – 10 weeks of age). Data reflect fold-change in IRF-8 levels relative to matched WT mice (first bar), and are expressed as the mean \pm SEM of three values. (B) Percentages of cell types in whole blood smear analysis. (C) CBC analysis; cell number ($\times 10^3$) graphed in log scale per μ l of sample. (D) Leukocyte analysis by flow cytometry. Data in A-C represent the mean \pm SEM of age- and gender (male)-matched WT and IRF-8-Tg mice (n = 5 mice/group).



Supplemental Figure 4. IRF-8 gain-of-function reduces MDSC subset generation. (A)

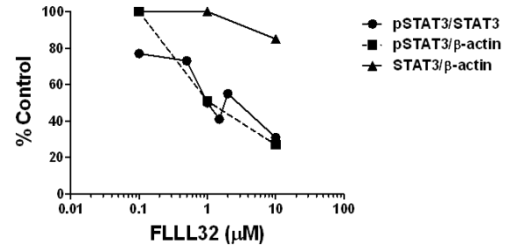
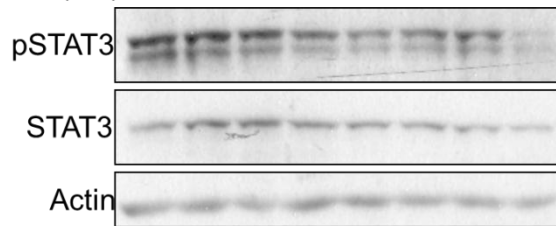
Spleens from representative AT-3 tumor-bearing WT or IRF-8-Tg mice (avg. tumor volume ~1500 mm³). (B) Flow plot of representative splenocytes of mice in A for the percentage of CD11b⁺Gr-1⁺ cells. (C) Data in B quantified (n=4 mice each, **P* < 0.03). (D) Data in C quantified for the percentages of monocytic or granulocytic subsets based on differential expression of Ly6C and Ly6G on the gated CD11b⁺ fraction (**P* < 0.05). (E) IRF-8 expression levels of splenic CD11b⁺Gr-1⁺ cells from the indicated groups. The results are presented as fold-change relative to the first column set at 1 (i.e., WT non-tumor-bearing control) (n=3 mice each, **P* < 0.01; NS=not significant). Data in C-E are presented as mean ± SEM of the indicated number of mice. (F) Representative density plots for the data quantified in Figure 7.



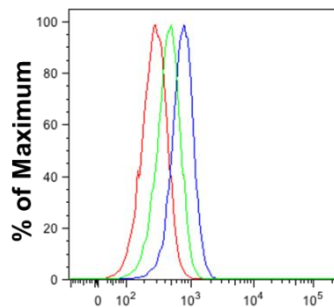
Supplemental Figure 5. Gating strategy for analyses of the different tumor-infiltrating myeloid populations. Analyses are based on the following approach: 1) total live cells were gated on the CD45⁺ leukocyte fraction; 2) the gated CD45⁺ fraction was then plotted in relation to CD11b and Gr-1 to identify total MDSCs (upper right); 3a) total CD11b⁺ cells were identified within the gated CD45⁺ fraction; 3b) the gated CD11b⁺ fraction was then plotted in relation to Ly6C and Ly6G to identify the MDSC subsets. The purple and blue gates spotlight the fractions analyzed, which represent the vast majority of cells within the respective quadrant; 3c) the gated CD11b⁺ fraction was also plotted in relation to F4/80 and Gr-1 to identify the macrophages (upper left); or 4) the gated CD45⁺ fraction was plotted in relation to CD11c and I-A^b (a major MHC class II molecule) to identify total DCs (upper right). Data are from a tumor-bearing WT mouse, although the same gating strategy was used for all tumor-bearing WT and Tg mice.

A. KG1a

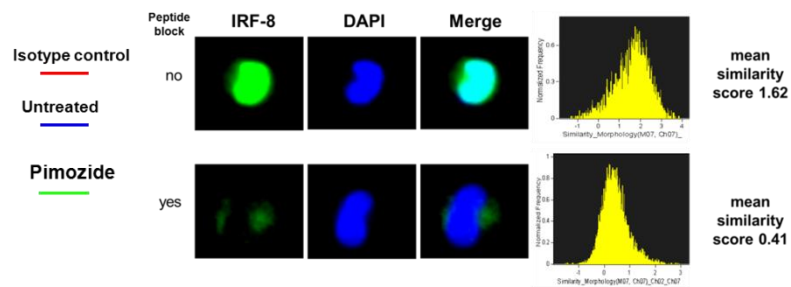
FLLL32 (uM): 0.0 0.1 0.5 1.0 1.5 2.0 5.0 10



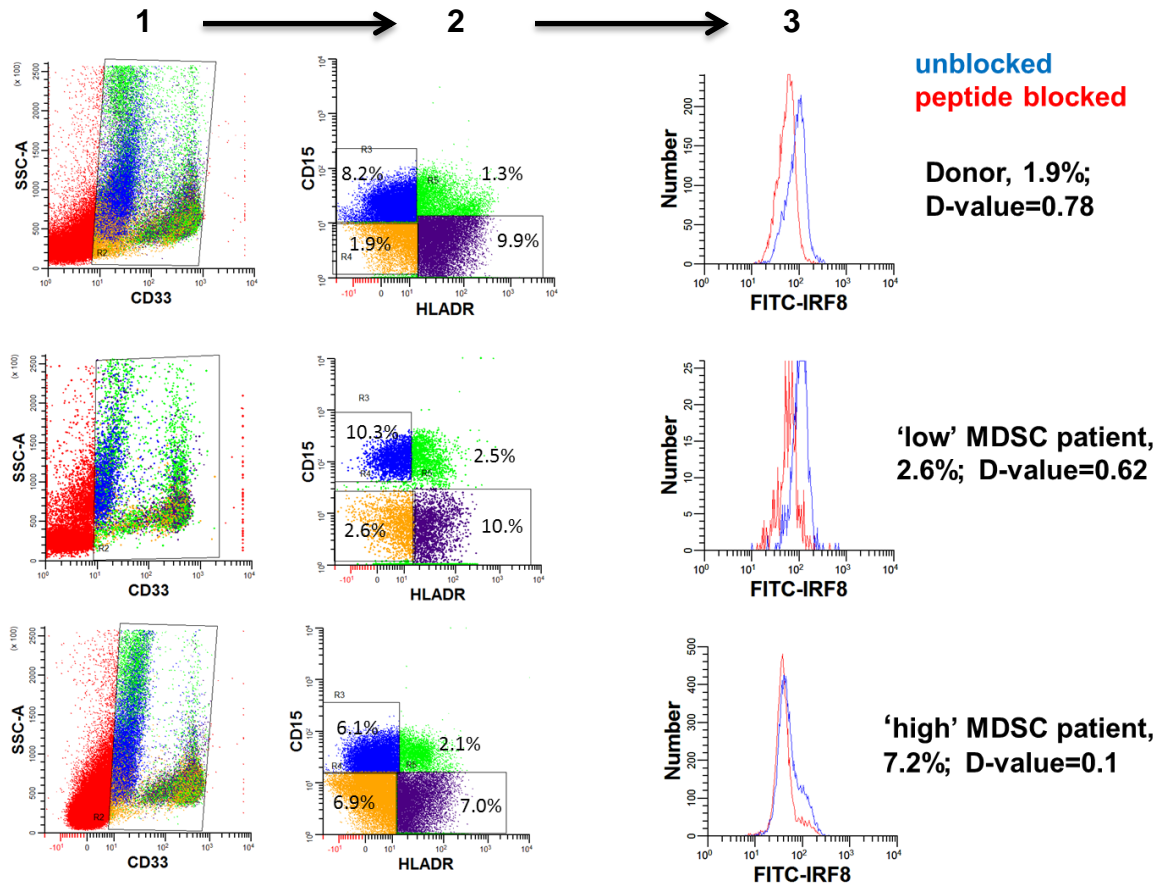
B. K562



C. THP-1



Supplemental Figure 6. Cell line models were used as positive controls for STAT3, STAT5 and IRF-8 analyses. (A) FLLL32 inhibits STAT3 phosphorylation in KG1a cells in a dose-dependent manner. KG1a cells were treated with the indicated concentrations of FLLL32 for 7 hours. Afterwards, STAT3 phosphorylation (phospho-STAT3 (Y705); Cell Signaling), as well as total STAT3 (Santa Cruz), and β-actin (Sigma) levels were measured by Western blot analysis (*left*) and densitometry (*right*). (B) Pimozide inhibits STAT5 phosphorylation in K562 cells, as measured by phospho-specific flow cytometry (Cell Signaling). K562 cells were treated with 10 μM pimozide (solid line, unfilled histogram), 1 μM imatinib (dashed line) or vehicle control (gray-filled histogram) for 3 hours. (C) IRF-8 expression by flow cytometry in IRF-8-expressing THP-1 cells. Intracellular IRF-8 staining of THP-1 cells was analyzed by Image Stream. Green represents IRF-8 staining; blue represents DAPI and teal represents the merge. Data illustrated as a similarity score. Random selected images of THP-1 cells showing IRF-8 localization, without (top) and with (bottom) peptide block.



Supplemental Figure 7. Gating strategy for the analysis of IRF-8 expression in the CD33⁺CD15⁻HLA-DR⁻ MDSC subset Buffy coat leukocytes from representative subjects (healthy donor or patients with low or high MDSC levels, as defined in Figure 10) were stained for expression of CD33, CD15, HLA-DR and IRF-8. Next, 1) live cells were gated on the CD33⁺ fraction; 2) CD33⁺ cells from each group were plotted in relation to CD15 and HLA-DR expression to identify the CD33⁺CD15⁻HLA-DR⁻ fraction (in the lower left quadrant); and 3) the gated CD33⁺CD15⁻HLA-DR⁻ fraction was then analyzed for IRF-8 expression. To do so, during the primary antibody incubation step, duplicate samples were prepared and incubated with or without an IRF-8 Ab blocking peptide to improve accuracy for IRF-8 quantification. Specific IRF-8 levels were then quantified using KS statistics and the data reported as the D-value as described in detail in the Methods.

Table I. Gene Set Enrichment Analysis: IRF-8^{-/-} vs. Wild-type Controls ^a

<u>GENE SET</u>	<u>#GENES</u>	<u>FDR.q.val^b</u>
MORI_IMMATURE_B_LYMPHOCYTE_DN	40	0
MORI_LARGE_PRE_BII_LYMPHOCYTE_UP	43	0
MARKEY_RB1_ACUTE_LOF_DN	144	0
HOFFMANN_LARGE_TO_SMALL_PRE_BII_LYMPHOCYTE_UP	69	0
YU_MYC_TARGETS_UP	29	0
BERENJENO_TRANSFORMED_BY_RHOA_UP	334	0
PAL_PRMT5_TARGETS_UP	116	0
LIAN_LIPA_TARGETS_6M	53	0
LIAN_LIPA_TARGETS_3M	47	0
ICHIBA_GRAFT_VERSUS_HOST_DISEASE_D7_UP	79	0
MARKEY_RB1_ACUTE_LOF_UP	171	0
HESS_TARGETS_OF_HOXA9_AND_MEIS1_DN	69	0
MARKEY_RB1_CHRONIC_LOF_DN	71	0
ZHANG_BREAST_CANCER_PROGENITORS_UP	229	0.00011
LE_EGR2_TARGETS_UP	62	0.000124
YAO_TEMPORAL_RESPONSE_TO_PROGESTERONE_CLUSTER_13	136	0.000496
RIZ_ERYTHROID_DIFFERENTIATION	50	0.000632
FOSTER_INFLAMMATORY_RESPONSE_LPS_DN	235	0.000865
GOLDRATH_ANTIGEN_RESPONSE	249	0.001154
SEKI_INFLAMMATORY_RESPONSE_LPS_UP	46	0.001165
MORI_EMU_MYC_LYMPHOMA_BY_ONSET_TIME_UP	76	0.001523
IVANOVA_HEMATOPOIESIS_EARLY_PROGENITOR	73	0.001818
STARK_PREFRONTAL_CORTEX_22Q11_DELETION_DN	355	0.002661
MARKEY_RB1_CHRONIC_LOF_UP	53	0.002706
VARELA_ZMPSTE24_TARGETS_UP	24	0.002838
OUELLET_OVARIAN_CANCER_INVASIVE_VS_LMP_UP	68	0.003657
MORI_MATURE_B_LYMPHOCYTE_DN	41	0.005326
MORI_MATURE_B_LYMPHOCYTE_UP	62	0.007333
BOYLAN_MULTIPLE_MYELOMA_PCA1_UP	55	0.013204
COATES_MACROPHAGE_M1_VS_M2_UP	42	0.013265
MORI_PRE_BI_LYMPHOCYTE_DN	54	0.013494
MORI_LARGE_PRE_BII_LYMPHOCYTE_DN	43	0.016997
BREDEMEYER_RAG_SIGNALING_NOT_VIA_ATM_UP	35	0.017263
MORI_IMMATURE_B_LYMPHOCYTE_UP	38	0.017823
MARTORIATI_MDM4_TARGETS_NEUROEPITHELIUM_DN	33	0.017885
ICHIBA_GRAFT_VERSUS_HOST_DISEASE_35D_UP	111	0.026818
YU_MYC_TARGETS_DN	45	0.02719
HOFFMANN_IMMATURE_TO_MATURE_B_LYMPHOCYTE_UP	19	0.027731
YAO_TEMPORAL_RESPONSE_TO_PROGESTERONE_CLUSTER_5	19	0.028404
YAO_HOXA10_TARGETS_VIA_PROGESTERONE_UP	37	0.031785
YAO_TEMPORAL_RESPONSE_TO_PROGESTERONE_CLUSTER_14	97	0.032518
MCBRYAN_PUBERTAL_BREAST_4_5WK_UP	100	0.036288

^a Refer to Figure 3 for experimental details; ^b FDR, false discovery rate

Table II Gene Set Enrichment Analysis: Tumor-Bearers vs. Wild-type Controls

<u>GENE SET</u>	<u>#GENES</u>	<u>FDR.q.val</u>
MORI_IMMATURE_B_LYMPHOCYTE_DN	40	0
HOFFMANN_LARGE_TO_SMALL_PRE_BII_LYMPHOCYTE_UP	69	0
MARKEY_RB1_ACUTE_LOF_DN	144	0
PAL_PRMT5_TARGETS_UP	116	0
YU_MYC_TARGETS_UP	29	0
MORI_LARGE_PRE_BII_LYMPHOCYTE_UP	43	0
YAO_TEMPORAL_RESPONSE_TO_PROGESTERONE_CLUSTER_13	136	0
BERENJENO_TRANSFORMED_BY_RHOA_UP	334	0
STARK_PREFRONTAL_CORTEX_22Q11_DELETION_DN	355	0
YAO_TEMPORAL_RESPONSE_TO_PROGESTERONE_CLUSTER_17	126	0
GOLDRATH_ANTIGEN_RESPONSE	249	0
IVANOVA_HEMATOPOIESIS_EARLY_PROGENITOR	73	0
SEKI_INFLAMMATORY_RESPONSE_LPS_UP	46	0
ICHIBA_GRAFT_VERSUS_HOST_DISEASE_D7_UP	79	0
MARKEY_RB1_ACUTE_LOF_UP	171	0
VARELA_ZMPSTE24_TARGETS_UP	24	0
RASHI_RESPONSE_TO_IONIZING_RADIATION_1	32	0
YAO_TEMPORAL_RESPONSE_TO_PROGESTERONE_CLUSTER_14	97	6.34E-05
LE_EGR2_TARGETS_UP	62	6.82E-05
OUELLET_OVARIAN_CANCER_INVASIVE_VS_LMP_UP	68	0.000131
ZHANG_BREAST_CANCER_PROGENITORS_UP	229	0.000301
ICHIBA_GRAFT_VERSUS_HOST_DISEASE_D7_DN	19	0.000462
MORI_EMU_MYC_LYMPHOMA_BY_ONSET_TIME_UP	76	0.000496
LEE_LIVER_CANCER_MYC_UP	26	0.0006
YAO_TEMPORAL_RESPONSE_TO_PROGESTERONE_CLUSTER_10	45	0.000631
HESS_TARGETS_OF_HOXA9_AND_MEIS1_DN	69	0.000636
IVANOVA_HEMATOPOIESIS_LATE_PROGENITOR	104	0.000759
FOSTER_INFLAMMATORY_RESPONSE_LPS_DN	235	0.000986
MORI_MATURE_B_LYMPHOCYTE_DN	41	0.001182
IVANOVA_HEMATOPOIESIS_INTERMEDIATE_PROGENITOR	26	0.001597
YAO_TEMPORAL_RESPONSE_TO_PROGESTERONE_CLUSTER_11	68	0.002257
RIZ_ERYTHROID_DIFFERENTIATION	50	0.002443
RASHI_RESPONSE_TO_IONIZING_RADIATION_2	86	0.003557
LIAN_LIPA_TARGETS_6M	53	0.00369
HOFFMANN_IMMATURE_TO_MATURE_B_LYMPHOCYTE_UP	19	0.003827
LIAN_LIPA_TARGETS_3M	47	0.004306
MODY_HIPPOCAMPUS_PRENATAL	19	0.005393
BREDEMEYER_RAG_SIGNALING_NOT_VIA_ATM_UP	35	0.008435
MORI_PRE_BI_LYMPHOCYTE_DN	54	0.009138
MORI_MATURE_B_LYMPHOCYTE_UP	62	0.010733
BOYLAN_MULTIPLE_MYELOMA_C_D_UP	64	0.010875
MARKEY_RB1_CHRONIC_LOF_UP	53	0.013204
SWEET_LUNG_CANCER_KRAS_DN	157	0.017183
MARTORIATI_MDM4_TARGETS_NEUROEPITHELIUM_UP	62	0.017396
BYSTRYKH_HEMATOPOIESIS_STEM_CELL_QTL_CIS	96	0.021923
MARKEY_RB1_CHRONIC_LOF_DN	71	0.024658
YU_MYC_TARGETS_DN	45	0.024977
MORI_PLASMA_CELL_UP	24	0.030429

Table II. Cont'd

LEE_LIVER_CANCER_E2F1_DN	23	0.030608
LIANG_HEMATOPOIESIS_STEM_CELL_NUMBER_LARGE_VS_TINY_UP	30	0.033018
CADWELL_ATG16L1_TARGETS_UP	35	0.038606
YAO_TEMPORAL_RESPONSE_TO_PROGESTERONE_CLUSTER_1	37	0.040275
YAO_TEMPORAL_RESPONSE_TO_PROGESTERONE_CLUSTER_5	19	0.040616
KUMAR_TARGETS_OF_MLL_AF9_FUSION	215	0.04451
COATES_MACROPHAGE_M1_VS_M2_UP	42	0.046538
RIZ_ERYTHROID_DIFFERENTIATION_CCNE1	26	0.047368
BERENJENO_ROCK_SIGNALING_NOT_VIA_RHOA_DN	28	0.048474

Table III. Gene Set Enrichment Analysis: IRF-8^{-/-} vs. Tumor-Bearers

<u>GENE SET</u>	<u>#GENES</u>	<u>FDR.q.val</u>
YAO_TEMPORAL_RESPONSE_TO_PROGESTERONE_CLUSTER_17	126	0
RASHI_RESPONSE_TO_IONIZING_RADIATION_1	32	0.001824
SEKI_INFLAMMATORY_RESPONSE_LPS_UP	46	0.002233
LIAN_LIPA_TARGETS_6M	53	0.006676
LIAN_LIPA_TARGETS_3M	47	0.007541
RAMALHO_STEMNESS_DN	50	0.008136
YAO_TEMPORAL_RESPONSE_TO_PROGESTERONE_CLUSTER_10	45	0.008429
MARKEY_RB1_CHRONIC_LOF_DN	71	0.008893
ICHIBA_GRAFT_VERSUS_HOST_DISEASE_D7_DN	19	0.009216
RASHI_RESPONSE_TO_IONIZING_RADIATION_2	86	0.010399
BOYLAN_MULTIPLE_MYELOMA_C_CLUSTER_DN	19	0.022165
LEE_LIVER_CANCER_MYC_UP	26	0.025036
ICHIBA_GRAFT_VERSUS_HOST_DISEASE_35D_UP	111	0.026649
YAO_TEMPORAL_RESPONSE_TO_PROGESTERONE_CLUSTER_9	45	0.030161
MARTORIATI_MDM4_TARGETS_NEUROEPITHELIUM_DN	33	0.03433
HOFFMANN_IMMATURE_TO_MATURE_B_LYMPHOCYTE_DN	20	0.035038
LEE_TARGETS_OF_PTCH1_AND_SUFU_UP	22	0.035181
MORI_IMMATURE_B_LYMPHOCYTE_DN	40	0.039157

Table IV. Characterization of bone marrow progenitors from CD11b-IRF8 transgenic mice *

Cell type	Wild-type mouse #			IRF-8 transgenic mouse #		
	1	2	3	1	2	3
Monocyte lineage total:	3%	4%	5%	6%	4%	3%
Monoblasts	0%	0%	0%	0%	0%	0%
Promonocytes	0%	0%	0%	0%	0%	0%
Monocytes	3%	4%	5%	6%	4%	3%
Platelet lineage total:	0%	1%	1%	0%	0%	1%
Megakaryoblasts	0%	0%	0%	0%	0%	0%
Megakaryocytes	0%	1%	1%	0%	0%	1%
Neutrophil lineage total:	28%	27%	32%	26%	26%	32%
Myeloblasts	0%	0%	0%	0%	0%	0%
Promyelocytes	3%	3%	3%	4%	1%	7%
Myelocytes	22%	19%	22%	16%	18%	17%
Metamyelocytes	3%	5%	5%	6%	5%	6%
Mature neutrophils	1%	1%	1%	1%	3%	2%
Eosinophil lineage total:	1%	5%	1%	3%	4%	2%
Myeloblasts	0%	0%	0%	0%	1%	0%
Promyelocytes	0%	1%	1%	1%	2%	1%
Myelocytes	1%	4%	1%	3%	2%	2%
Metamyelocytes	0%	1%	0%	0%	0%	0%
Cell type	Wild-type mouse #			IRF-8 transgenic mouse #		
	1	2	3	1	2	3
Indeterminant myeloblasts:	6%	1%	2%	5%	4%	4%
Erythroid lineage total:	63%	51%	31%	41%	44%	45%
Erythroblast	2%	4%	1%	4%	2%	4%
Proerythroblasts	1%	2%	2%	2%	3%	3%
Basophilic erythroblasts	4%	2%	2%	1%	5%	2%
Polychromatic erythroblasts	3%	5%	3%	6%	3%	5%
Orthochromatic erythroblasts	7%	3%	5%	4%	3%	3%
Erythrocytes/reticulocytes:	46%	38%	16%	26%	30%	30%
Lymphoid lineage total:	17%	11%	13%	17%	13%	13%
Lymphoblasts	0%	0%	0%	0%	0%	0%
Polymorphoblasts	0%	0%	0%	0%	0%	0%
Lymphocytes	17%	11%	13%	17%	13%	13%
Plasma cell lineage total:	1%	1%	2%	1%	2%	0%
Plasmablasts	0%	0%	0%	0%	0%	0%
Proplasma cells	0%	0%	1%	1%	1%	0%
Plasmacells	1%	1%	1%	1%	1%	0%
Unidentified blast cells:	1%	2%	4%	2%	3%	2%

* Analysis of bone marrow progenitors of the various lineages between WT and IRF-8-Tg transgenic under steady state-conditions (founder line 370; n=3 mice each). Morphological analysis was conducted in a blinded fashion.

Table V. Demographic and Clinical Characteristics of the Breast Cancer Patient Population

<u>Patient Characteristics</u>		<u>Number of Patients (n=30)</u>
Age (years)	Median	59
	Average (\pm SEM)	59.6 ± 3.0
	Range	39 – 86
Race	Caucasian	28
	African American	1
	Hispanic	1
Histology	Invasive ductal	23
	Invasive lobular	7
Stage	IIIA	12
	IIIB	3
	IIIC	9
	IV	6
Tumor Size (cm)	< 2	6
	2-5	11
	> 5	11
	Not provided	2
Tumor grade	1	0
	2	2
	3	27
	Data not provided	1
Triple-negative	Yes	8
	No	22
Non-triple-negative (n=22)	ER+/PR+/Her2+	1
	ER+/PR+/Her2-	13
	ER+/PR-/Her2+	1
	ER+/PR-/Her2-	2
	ER-/PR-/Her2+	5
Lymph nodes Positive	None	4
	Data not provided	1
	Yes	25
	Median	6
	Average (\pm SEM)	7.4 ± 1.3
Range	1 – 27	